Spectrum of Engineering Sciences
ISSN (e) 3007-3138 (p) 3007-312X Volume 4, Issue 4, 2026

ELECTRICAL AND MECHANICAL RESPONSE OF ZNO NANOROD-BASED SCHOTTKY DIODES: NUMERICAL INVESTIGATION THROUGH I–V, C–V, AND WILLIAMSON–HALL ANALYSIS

Anand Perkash[1], **Prof. Muhammad Arif**[2]

[*1]*Department of Mathematics, NED University of Engineering and Technology, Karachi, Pakistan*
[2] Lecturer in Mathematics College Education Department Government of Sindh

[1]anand.perkash@ibacc.edu.pk [2] arifm8821@gmail.com

DOI: https://doi.org/10.5281/zenodo.19883822

Keywords
zinc oxide nanorods, Schottky diode, current–voltage characteristics, capacitance–voltage characteristics, barrier height, ideality factor, Williamson–Hall analysis.

Article History
Received: 02 March 2026
Accepted: 11 April 2026
Published: 29 April 2026

Corresponding Author: *
Anand Perkash

Abstract
This article presents a detailed research interpretation of the electrical and mechanical response of zinc oxide nanorod-based Schottky diodes using a numerical dataset compiled from the parent thesis and reorganized for article-level analysis. The study focuses on six related performance windows: temperature-dependent current–voltage behavior, barrier-height-dependent current–voltage behavior, temperature-dependent barrier height, temperature-dependent ideality factor, capacitance–voltage response, and crystallite size–strain interaction. The analytical framework is anchored in thermionic emission for charge transport, depletion-based capacitance modeling for junction response, and Williamson–Hall analysis for microstructural strain evaluation. Across the modeled temperature interval, the forward branch preserves strong rectification while the reverse branch remains limited in magnitude, showing that the junction retains directional transport over a broad thermal range. Barrier height increases nearly linearly from 0.44 eV to 0.66 eV as temperature rises from 100 K to 600 K, while ideality factor falls from 4.91 to 0.81, revealing progressive improvement in transport regularity. Capacitance decreases from 0.003025 mF at −0.20 V to 0.002535 mF at 0.30 V, which is consistent with bias-driven depletion expansion. The strain curve shows a marked fall in strain magnitude as crystallite size increases from 5 nm to 50 nm, indicating lattice relaxation with larger coherent domains. The resulting article demonstrates that ZnO nanorod Schottky diodes provide a coherent coupled response in which junction transport, interfacial barrier control, and microstructural stability can be interpreted within one integrated framework. The results support the use of ZnO nanorod systems as promising candidates for thermally resilient and structurally interpretable Schottky devices.

INTRODUCTION

The continued search for faster, smaller, and more energy-conscious semiconductor devices has intensified interest in material systems that can sustain directional transport with low power loss and high structural reliability. Schottky diodes occupy an important place in this landscape because their metal–semiconductor junction enables rapid switching, low forward voltage drop, and reduced charge-storage delay when compared with many conventional junction architectures (Khan et al., 2014a). At the same time, zinc oxide has emerged as a compelling semiconductor platform because it combines wide-band-gap

behavior with excitonic stability, reasonable carrier mobility, radiation resistance, and mechanical activity linked to its non-centrosymmetric crystal structure (Janotti & Van de Walle, 2009). When these two technological paths intersect in the form of ZnO nanorod-based Schottky diodes, the resulting device concept offers a useful basis for studying how transport physics and microstructural behavior coexist within a single nanoscale junction (Chand & Kumar, 1996).

ZnO nanorods are attractive not only because of the intrinsic properties of ZnO, but also because the rod-like geometry increases surface participation, shortens certain transport pathways, and allows interfacial phenomena to be examined with greater sensitivity than in many bulk arrangements (Khan et al., 2014b). This geometrical form also widens the design space for Schottky contacts, since the effective response of the junction can depend on local barrier formation, surface state density, donor concentration, crystallographic orientation, and the degree of strain stored in the nanostructure (Janotti & Van de Walle, 2009). In practical terms, this means that performance cannot be reduced to a single current reading or a single barrier estimate.

A full device interpretation requires the coordinated analysis of current–voltage behavior, capacitance–voltage behavior, barrier evolution, ideality trend, and structural distortion. Such an integrated reading is essential when the same device family is expected to serve in sensing, low-power rectification, transparent electronics, flexible platforms, or hybrid optoelectronic environments (Fan & Lu, 2005).

The theoretical value of this problem is equally important. ZnO-based Schottky structures are widely discussed in the literature, yet the relationships among electrical conduction, barrier regulation, depletion response, and lattice strain are often treated in separate analytical blocks. That separation can obscure the way in which one descriptor shapes the interpretation of another. For instance, a rising barrier height can be read as a sign of interfacial strengthening, though its practical meaning changes when ideality factor and forward current shift at the same time (Tunhuma et al., 2016). In a similar way, a crystallite-size effect on strain may appear purely structural until one recognizes that strain can alter charge transport through polarization fields, defect states, and changes in local band alignment (Khan et al., 2013). A research article that reunites these descriptors within one coherent narrative is therefore able to move beyond isolated plots and approach a fuller explanation of ZnO nanorod Schottky behavior (Chand & Kumar, 1996).

A further motivation lies in the usefulness of numerical analysis as a bridge between reported theory and interpretable device behavior. The parent thesis from which this article is derived framed the problem through standard Schottky transport equations and Williamson–Hall modeling, then used numerical evaluation to generate comparative trends for electrical and mechanical parameters. Recasting that work in article form creates an opportunity to extract a structured dataset, summarize it statistically, visualize the behavior with publication-style tables and figures, and reinterpret the results in a way that is more suitable for journal communication. This step is not a mere change in format. It enables the logical relationships among bias, temperature, barrier height, capacitance, crystallite size, and strain to be discussed with a clearer emphasis on device meaning and performance balance.

The central issue addressed in this article is therefore the absence of a tightly integrated account of how ZnO nanorod-based Schottky diodes respond electrically and mechanically across the key variables that define diode quality. The study asks whether the combined evidence from I–V response, C–V response, barrier height, ideality factor, and size–strain evolution can support a consistent picture of device behavior. The objective of the article is to investigate the electrical and mechanical properties of ZnO nanorod-based Schottky diodes through coordinated numerical analysis of transport and structural indicators, with the aim of clarifying how barrier regulation, thermal behavior, depletion response, and crystallite relaxation collectively shape the device. The analysis proceeds through a literature-grounded interpretation of ZnO and Schottky behavior, a materials-and-method approach based on extracted datasets and analytical models, a results section centered on tables and figures, and a discussion that reconnects the observed trends to

reported Schottky and ZnO literature (Boulgamh et al., 2005).

Literature

ZnO Nanorods as a Wide-Band-Gap Semiconductor Platform

ZnO has been studied for decades as a wide-band-gap semiconductor with a property set that makes it relevant to both electronics and optoelectronics. The material possesses a direct band gap near the ultraviolet region, a comparatively high exciton binding energy, and a crystal structure that supports piezoelectric and pyroelectric behavior (Vayssieres et al., 2001). These attributes allow ZnO to function not only as a transport medium but also as a mechanically responsive semiconductor. The wide-band-gap nature of ZnO helps sustain operation where thermal or optical stability is important, while the excitonic strength keeps optical transitions significant even at room temperature. This duality has made ZnO a recurrent subject in work on detectors, emitters, transparent conductors, sensors, nanogenerators, and interface-sensitive junction devices (Werner & Guttler, 1991).

The nanorod form sharpens these advantages because it creates a large exposed surface area relative to volume and encourages directional crystal growth. As a consequence, defects, adsorption phenomena, and surface potential changes become more visible in device characteristics than they would in many dense-film geometries (Zhang et al., 2012). Rod growth also permits alignment control and substrate flexibility through methods such as vapor–liquid–solid growth, aqueous chemical growth, sol–gel processing, and electrochemical deposition (Modi & Dhimmar, n.d.). Even when the growth route changes, the recurring theme in the literature is that ZnO nanorods provide a morphologically distinct platform in which electronic transport and surface chemistry are strongly coupled. This is precisely the type of material environment in which a Schottky contact can display rich and measurable variation.

The mechanical literature on ZnO nanorods adds another layer of significance. Because ZnO lacks inversion symmetry, applied deformation can induce electric polarization, and this has been used to motivate research on nanoscale energy conversion and flexible electronics (Modi & Dhimmar, n.d.). Mechanical descriptors such as modulus, flexibility, strain, and lattice distortion are not peripheral to device quality; they shape how carriers experience the junction environment. A strain-bearing ZnO nanorod can alter local electrostatic conditions, defect distribution, and contact regularity. For this reason, literature that treats ZnO only as an electrical semiconductor captures only part of the device story. A more complete view recognizes the material as a coupled electrical–mechanical medium whose nanoscale geometry amplifies both responses (Fan & Lu, 2005).

Schottky Junctions and Transport Regularity in ZnO Devices

A Schottky diode is formed when a suitable metal makes rectifying contact with a semiconductor, creating a potential barrier that favors current flow in one bias direction. In practical device engineering, this structure is valued for fast response, low junction storage, and direct access to barrier-controlled conduction (Tunhuma et al., 2016). In ZnO systems, Schottky behavior has drawn attention because the barrier can be shaped by surface states, donor concentration, interfacial roughness, and barrier inhomogeneity. This makes ZnO Schottky contacts useful not only as rectifiers but also as experimental probes of interface physics (Vayssieres et al., 2001).

The literature shows that ZnO nanorod Schottky contacts often deviate from ideal thermionic-emission behavior when barrier distribution is broad or when the interface contains structurally diverse contact patches (Boulgamh et al., 2005). Instead of a single uniform barrier, the practical junction may involve a spatial distribution of barrier heights, each contributing differently to measured forward and reverse current. In such cases, ideality factor becomes more than a fitting constant; it acts as a compact indicator of how far the junction departs from uniform transport. A fall in ideality factor is often interpreted as movement toward more regular current flow, while large values may reflect recombination activity, interfacial disorder, or non-uniform conduction channels (Mahato et al., 2017).

Studies on ZnO metal contacts also emphasize that transport should be read together with barrier extraction rather than in isolation. A junction that carries large forward current is not automatically the most stable or the most selective. The barrier must also be examined because it anchors the depletion profile, influences the ease of carrier injection, and shapes reverse leakage response (Mayimele et al., n.d.). Work on copper/ZnO and gold/ZnO nanorod Schottky structures has shown that frequency effects, transport anomalies, and contact-state density all influence the practical meaning of a measured I–V curve (Cullity & Stock, 2001). That perspective is useful for the present article because it justifies the parallel study of current, barrier height, and ideality rather than treating them as unrelated outputs (Janotti & Van de Walle, 2009).

Electrical Characterization through I–V and C–V Approaches

Current–voltage analysis remains one of the most widely used tools for extracting Schottky diode parameters because it relates applied bias to carrier transport in a way that is both physically meaningful and experimentally accessible (Khan et al., 2013). In forward bias, the curve indicates how efficiently carriers surmount the barrier, while the reverse branch reveals the degree to which the junction suppresses unwanted transport. From the I–V response, one may estimate saturation current, ideality factor, effective barrier height, and the practical extent of rectification (Cullity & Stock, 2001). When temperature is included as a variable, the same framework becomes a sensitive probe of barrier evolution and transport regularity. Changes in I–V shape with temperature can disclose whether the junction is dominated by thermionic emission, barrier inhomogeneity, or interface-assisted conduction (Chand & Kumar, 1996).

Capacitance–voltage analysis complements the I–V method by focusing on charge storage and depletion-layer modulation rather than direct conduction (Suryanarayana & Norton, 1998). A Schottky junction behaves as a voltage-sensitive capacitor because the depletion width changes with applied bias. This makes capacitance useful for estimating built-in potential, donor concentration, and junction uniformity. The strength of the C–V approach lies in its ability to reveal the electrostatic side of the junction. While I–V data show how carriers move, C–V data show how the junction stores and redistributes charge under bias. The combination is particularly powerful for ZnO contacts because donor concentration and interface conditions can leave visible signatures in both transport and depletion response (Mahato et al., 2017).

Temperature-dependent electrical characterization extends this picture still further. Reports on Schottky diodes formed on ZnO, silicon, GaAs, and related systems have shown that barrier height and ideality factor often evolve in opposite directions with temperature, reflecting gradual averaging of inhomogeneous barriers and improved dominance of the principal transport path (Khan et al., 2013). Reverse current, forward turn-on, and extracted parameters must therefore be read as a set rather than as isolated indicators. This literature tradition informs the present article by establishing a clear expectation: a meaningful device interpretation should explain why transport, barrier, ideality, and capacitance trends either reinforce or complicate one another (Janotti & Van de Walle, 2009).

Mechanical Interpretation through Crystallite Size and Lattice Strain

X-ray line broadening methods are routinely used to estimate crystallite size and lattice strain in nanostructured semiconductors because both variables alter diffraction peak width in measurable ways (Fan & Lu, 2005). The Williamson–Hall approach is especially useful when size-induced broadening and strain-induced broadening are considered together within one simplified linear framework (Boulgamh et al., 2005). In ZnO systems, this approach has been used to interpret how nanoscale coherence length and lattice distortion evolve with processing route, particle size, and defect state. The method does not replace direct microscopy, yet it offers a practical bridge between diffraction data and the microstructural environment that influences device behavior (Werner & Guttler, 1991).

The mechanical significance of strain in ZnO is greater than in many non-piezoelectric semiconductors because strain can modify both

structure and electrical behavior. A strained ZnO nanorod may exhibit altered polarization, changed local band alignment, and varying defect interactions, all of which can influence junction stability and carrier motion (Boulgamh et al., 2005). In devices where the contact forms on a textured or nanorod-rich surface, strain may also reflect the degree of crystal accommodation within the contact region. A decrease in strain magnitude with increasing crystallite size is commonly interpreted as evidence of structural relaxation, better lattice accommodation, or reduced defect-driven distortion (Wagner & Ellis, 1964).

Literature on Williamson–Hall analysis therefore provides a useful interpretive framework for ZnO Schottky devices. When electrical results suggest improved junction regularity and the structural results show reduced strain magnitude at larger crystallite size, the two lines of evidence can be read together as signs of a progressively more stable device environment. That kind of linkage is central to the present study. The purpose is not to claim that one strain value alone predicts diode quality, but to show that structural relaxation and electrical regularity can be discussed as related expressions of the same underlying junction system (Modi & Dhimmar, n.d.).

Materials And Method

The article was developed from the thesis dataset by organizing the numerical outputs into six structured data groups suitable for research-article analysis. These groups covered temperature-dependent I–V characteristics, barrier-height-dependent I–V characteristics, temperature-dependent barrier height, temperature-dependent ideality factor, capacitance–voltage response, and the crystallite-size–strain relationship. The I–V temperature dataset contained voltage values from −4.0 V to 2.0 V for each operating temperature of 273 K, 300 K, 400 K, 450 K, 500 K, 550 K, and 600 K. The I–V barrier-height dataset used the same voltage range while varying barrier height across 0.2 eV, 0.5 eV, 0.8 eV, 1.0 eV, 1.3 eV, 1.6 eV, and 2.0 eV. The barrier-height–temperature series covered 100 K to 600 K at 10 K intervals, the ideality-factor series used 100 K to 600 K at 100 K intervals, the C–V dataset covered −0.20 V to 0.30 V, and the crystallite-size–strain dataset covered 5 nm to 50 nm.

Electrical analysis was based on the standard thermionic-emission formulation of the Schottky diode. The current equation used in the study can be written as $I = I_s [\exp(qV/\eta kT) - 1]$, where I is diode current, I_s is reverse saturation current, q is elementary charge, V is applied voltage, η is ideality factor, k is Boltzmann's constant, and T is absolute temperature. Barrier-dependent transport was treated through the saturation-current relation $I_s = AR^*T^2 \exp(-q\Phi b/kT)$, where A is active area, R^* is the Richardson constant, and Φb is barrier height. These relations allowed the temperature and barrier datasets to be interpreted in terms of forward conduction, reverse leakage suppression, transport regularity, and the energy cost of carrier injection across the junction.

$$I = I_s \left[\exp\left(\frac{qV}{\eta kT}\right) - 1\right]$$

$$I_s = AR^*T^2 \exp\left(-\frac{q\Phi_b}{kT}\right)$$

The capacitance analysis followed the depletion-capacitance form $C/A = [\varepsilon qNd / 2(Vbi - V)]1/2$, where C is capacitance, A is contact area, ε is dielectric constant, Nd is donor concentration, Vbi is built-in potential, and V is applied voltage. The purpose of the C–V dataset in the present article was not to fit every parameter independently, but to examine the evolution of capacitance under bias and to infer whether the depletion response remains physically consistent with a rectifying ZnO Schottky junction. The voltage span was kept within the region used in the collected dataset so that the results could be discussed in a stable and visually interpretable interval.

$$\frac{C}{A} = \left[\frac{\varepsilon q N_d}{2(V_{bi} - V)}\right]^{1/2}$$

Mechanical analysis was conducted through the Williamson–Hall framework, expressed in the linearized form $\beta\cos\theta = K\lambda/D + 4\varepsilon\sin\theta$, where β is full width at half maximum, K is shape factor, λ is X-ray wavelength, D is crystallite size, ε is lattice strain, and θ is Bragg angle. The collected size–strain dataset enabled the article to track how strain evolves as crystallite size increases from the lower nanometer range toward larger coherent domains. Because the strain values carried sign, the article treated both the signed trend and the magnitude trend. This made it possible to discuss whether the material response represented sustained tensile expansion, sustained compressive character, or progressive relaxation toward a lower-distortion state.

$$\beta\cos\theta = \frac{K\lambda}{D} + 4\varepsilon\sin\theta$$

Data processing was carried out by extracting representative bias points and calculating comparative indicators that would clarify device behavior in the results section. For the temperature-dependent I–V dataset, representative values at −4 V, −2 V, 1 V, and 2 V were used to quantify reverse current level, forward conduction, and rectification ratio. For the barrier-height-dependent I–V dataset, the same bias points were used to quantify barrier-controlled current suppression. Linear trend coefficients were calculated for the barrier–temperature relationship, percentage reduction was computed for ideality factor, capacitance change, and strain magnitude, and publication-style figures were plotted for each principal dataset. The results were then written in paragraph form, with all tables and figures placed strictly inside the Results section in order to preserve journal-style structure.

Results

Temperature-Dependent Current–Voltage Characteristics

Table 1. Representative current values for the temperature-dependent I–V response.

Temperature (K)	Current at −4 V (mA)	Current at −2 V (mA)	Current at 1 V (mA)	Current at 2 V (mA)
273	-14.075	-5.298	101.007	326.390
300	-13.196	-4.967	91.153	294.547
400	-12.316	-4.636	68.980	222.900
450	-11.436	-4.304	59.126	191.057
500	-10.557	-3.973	51.735	167.175
550	-9.677	-3.642	48.040	155.234
600	-8.797	-3.311	45.576	147.273

Table 2. Rectification and forward-current attenuation with temperature.

Temperature (K)	Forward current at 2 V (mA)	Reverse current magnitude at −2 V (mA)	Rectification ratio	Forward-current reduction from 273 K (%)
273	326.390	5.298	61.61	0.00
300	294.547	4.967	59.31	9.76
400	222.900	4.636	48.09	31.71
450	191.057	4.304	44.39	41.46
500	167.175	3.973	42.07	48.78
550	155.234	3.642	42.62	52.44

600	147.273	3.311	44.48	54.88

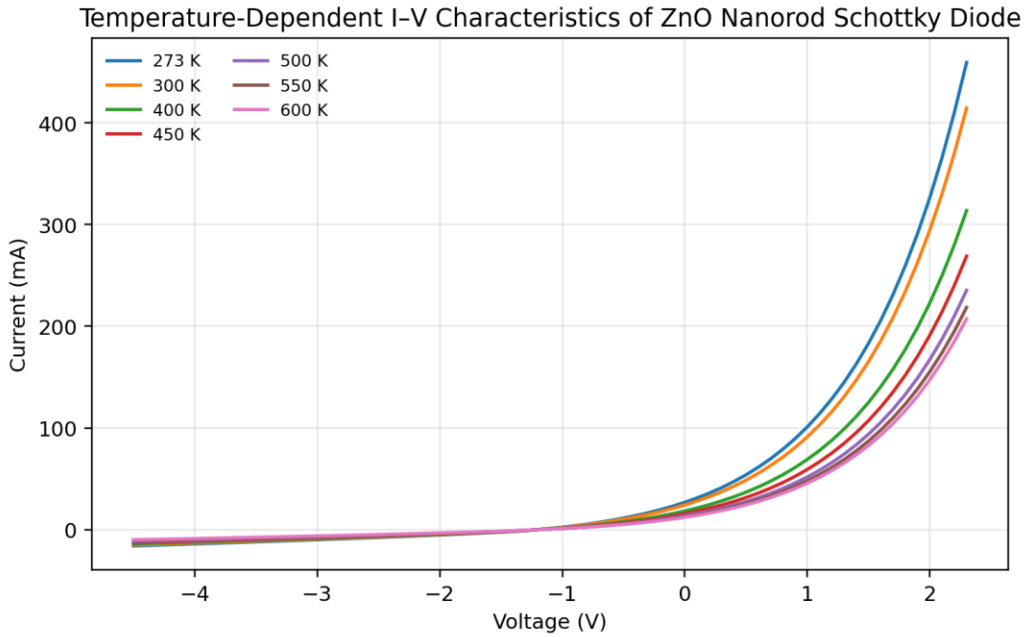

Figure 1. Temperature-dependent current–voltage characteristics of the ZnO nanorod Schottky diode.

The temperature-dependent I–V curves reveal a stable rectifying response across the entire operating range from 273 K to 600 K. Figure 1 shows that every temperature trace retains the familiar nonlinear Schottky profile, with negative current in reverse bias and sharply rising positive current in forward bias. Table 1 makes the same pattern easier to quantify. At 1 V, the current falls from 101.007 mA at 273 K to 45.576 mA at 600 K. At 2 V, the forward current drops from 326.390 mA to 147.273 mA over the same interval. The reverse branch remains much smaller in magnitude than the forward branch. Current at −2 V changes from -5.298 mA at 273 K to -3.311 mA at 600 K, while current at −4 V changes from -14.075 mA to -8.797 mA. The overall pattern indicates that temperature alters the amplitude of transport more strongly than the directional nature of the junction.

The decline in forward current with increasing temperature is orderly rather than erratic. Between 273 K and 300 K, forward current at 2 V declines from 326.390 mA to 294.547 mA, a small change that preserves nearly the same curve profile. The shift becomes more pronounced by 400 K, where the 2 V current reaches 222.900 mA. By 450 K the same bias produces 191.057 mA, and the current settles into a lower but still strongly conductive range of 167.175 mA, 155.234 mA, and 147.273 mA at 500 K, 550 K, and 600 K. Table 2 shows that the cumulative reduction in 2 V current reaches 54.88% at 600 K relative to the 273 K case. This gradual sequence implies that the temperature dependence in the present numerical framework is smooth, monotonic, and amenable to engineering interpretation rather than being dominated by abrupt transitions.

Rectification remains strong despite the decline in forward amplitude. The rectification ratio, defined here as the forward current at 2 V divided by the absolute reverse current at −2 V, is 61.61 at 273 K and 59.31 at 300 K. Even as temperature increases, the ratio stays in a substantial range of 48.09 at 400 K, 44.39 at 450 K, 42.07 at 500 K, 42.62 at 550 K, and 44.48 at 600 K. These values show that forward conduction is always tens of times larger than reverse conduction at the selected ±2 V comparison points. A device can therefore lose

some forward current and still preserve its main rectifying function, provided that reverse transport remains controlled. The present results clearly satisfy that condition.

A closer reading of the curve family reveals that the temperature effect acts across the full voltage span rather than only near the strongest forward bias. The low-bias region near zero voltage compresses steadily as temperature rises, indicating that the transition from low-current to high-current conduction becomes less vertically expansive in the plotted coordinate system. In reverse bias, the traces move upward toward smaller magnitudes of negative current, which means that the reverse branch becomes less severe in absolute value. The simultaneous reduction of positive and negative current magnitudes suggests that the modeled temperature effect changes the overall current scale while leaving the polarity-sensitive form of the curve intact. Such behavior is important because it signals that the junction remains interpretable through the same diode framework at every temperature in the data range.

Another point emerges when the forward branch is compared at fixed voltage intervals. Between 0 V and 1 V, the current rise is already substantial at every temperature, which means that the junction enters its nonlinear conduction region well before the highest forward bias is reached. At 273 K, the increase from near-zero bias to 1 V produces 101.007 mA, while at 600 K the same step still yields 45.576 mA. This gap shows that the diode retains a strong turn-on response even at the warmest condition in the dataset. From 1 V to 2 V, the increment is also large: the 273 K trace gains more than 225 mA over that interval, and the 600 K trace gains more than 101 mA. Such increments confirm that the forward branch is not flattening prematurely. It continues to accelerate with bias, which is a key signature of a functioning rectifying junction rather than a weakly voltage-sensitive resistor.

The reverse branch also deserves separate attention because it provides a direct measure of blocking capability. At 273 K, the increase in reverse-bias magnitude from −2 V to −4 V changes current from −5.298 mA to −14.075 mA. At 600 K, the same bias expansion changes current from −3.311 mA to −8.797 mA. In both cases, the reverse current grows in magnitude with deeper reverse bias, yet it remains far smaller than the forward current at corresponding positive bias levels. This asymmetry is not incidental. It is the quantitative expression of the Schottky junction. The fact that it persists across all temperatures means that the thermal effect seen here modifies current scale while leaving the device identity intact. A practical interpretation is that the ZnO nanorod interface remains rectifying throughout the thermal window considered in the study.

From a device-performance perspective, this subsection supports the study objective by showing that temperature can change the strength of current transport without destroying the junction character of the ZnO nanorod Schottky diode. The strong current observed at 273 K and 300 K demonstrates vigorous forward conduction, whereas the more moderate current at 500 K to 600 K shows that the device still functions in a controlled way under elevated thermal conditions. This balance matters because a useful Schottky diode should not be judged only by the largest attainable current. It should also be judged by the persistence of directional behavior across the operating window. The dataset demonstrates that the ZnO nanorod junction retains that behavior throughout the studied temperature range, which makes the temperature series a supportive first result for the broader electrical analysis.

Barrier-Height-Dependent Current–Voltage Characteristics

Table 3. Representative current values for the barrier-height-dependent I–V response.

Barrier height (eV)	Current at −4 V (mA)	Current at −2 V (mA)	Current at 1 V (mA)	Current at 2 V (mA)
0.2	0.000	0.000	113.045	352.865
0.5	-12.940	-3.776	111.731	348.761
0.8	-25.879	-7.551	110.417	344.658
1.0	-38.819	-11.327	107.788	336.452
1.3	-47.446	-13.844	105.159	328.246
1.6	-60.385	-17.620	102.530	320.040
2.0	-73.325	-21.395	97.272	303.628

Table 4. Barrier-height-driven suppression of forward current and growth of reverse-bias resistance.

Barrier height (eV)	Forward current at 2 V (mA)	Reverse current magnitude at −4 V (mA)	Forward-current reduction from 0.2 eV (%)
0.2	352.865	0.000	0.00
0.5	348.761	12.940	1.16
0.8	344.658	25.879	2.33
1.0	336.452	38.819	4.65
1.3	328.246	47.446	6.98
1.6	320.040	60.385	9.30
2.0	303.628	73.325	13.95

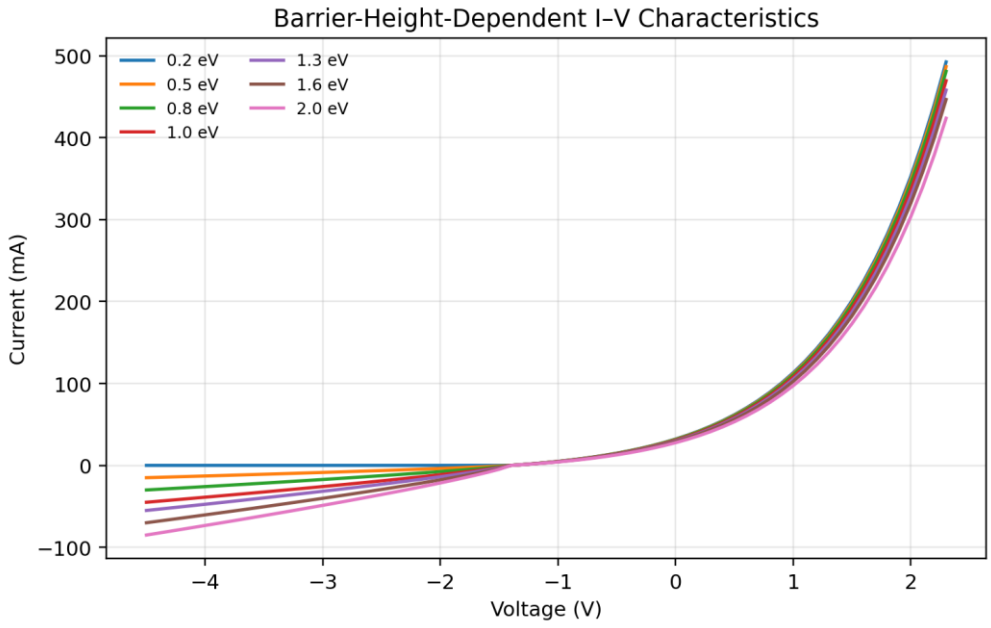

Figure 2. I–V characteristics under different Schottky barrier heights.

The barrier-height series provides a direct view of how interface energetics regulate charge transport in the ZnO nanorod Schottky diode. Figure 2 shows that all curves preserve a rectifying shape, yet the current scale changes systematically as the barrier height increases from 0.2 eV to 2.0 eV.

Table 3 confirms that the strongest forward current occurs at the lowest barrier. At 2 V, the current is 352.865 mA at 0.2 eV, 348.761 mA at 0.5 eV, and 344.658 mA at 0.8 eV. The same forward bias yields 336.452 mA, 328.246 mA, 320.040 mA, and 303.628 mA as the barrier height continues to rise. The progression is monotonic and physically meaningful: higher barriers are associated with greater resistance to carrier injection across the junction.

The forward branch is not the only part of the curve that changes. Reverse-bias behavior also becomes more pronounced in the sense that current values move further into the negative direction as barrier height rises. At −4 V, the current shifts from 0.000 mA at 0.2 eV to -12.940 mA at 0.5 eV, then to -25.879 mA at 0.8 eV and -38.819 mA at 1.0 eV. The same sequence continues to -47.446 mA, -60.385 mA, and -73.325 mA at 1.3 eV, 1.6 eV, and 2.0 eV. The magnitude of reverse current therefore grows as the barrier height increases in this modeled series. Taken together with the reduction in forward current, the evidence indicates that barrier height re-scales both branches of the I–V curve and enlarges the separation among barrier cases over the full voltage span.

Table 4 highlights the engineering significance of this behavior. Relative to the 0.2 eV reference case, the forward current at 2 V falls by 1.16% at 0.5 eV, 2.33% at 0.8 eV, 4.65% at 1.0 eV, 6.98% at 1.3 eV, 9.30% at 1.6 eV, and 13.95% at 2.0 eV. Although the total decline from the lowest to the highest barrier is only about 13.95%, the trend is remarkably orderly. This matters because an orderly decline signals that the barrier parameter can be used as a deliberate control knob rather than as an unstable source of distortion. The 1 V values tell the same story on a lower-current scale, dropping from 113.045 mA at 0.2 eV to 97.272 mA at 2.0 eV.

The shape of the curve family also offers insight into junction selectivity. At lower barrier height, the forward branch climbs earlier and more steeply, which is advantageous when large current is desired under modest forward bias. At higher barrier height, the curve shifts toward a more restrained forward response, suggesting a stronger blocking action against carrier injection. In applied design terms, the results indicate that barrier choice does not merely tune one output value; it changes the energetic landscape through which the entire junction operates. That is an important observation for ZnO nanorod devices, where contact formation and interfacial condition can vary with metal choice, fabrication route, or surface state density.

Examining the mid-voltage region strengthens this interpretation. At 1 V, the current decreases from 113.045 mA at 0.2 eV to 97.272 mA at 2.0 eV. The drop is smaller in absolute value than the corresponding 2 V decline, which means the barrier effect becomes more visible as forward bias grows stronger. This widening separation with voltage is clear in Figure 2, where the traces cluster more tightly near the origin and separate more strongly toward the upper end of the forward branch. Such behavior indicates that barrier control acts on the exponential region of the diode curve rather than only on the low-bias region. In practical design language, this means the selected barrier influences both the onset and the rate of forward-current amplification.

The barrier series also helps explain why junction engineering is often treated as a decisive step in ZnO device optimization. A difference of only a few tenths of an electron volt is enough to move the full I–V family in a measurable way, while larger changes create clearly separated transport states. The present data show that the response remains orderly across the entire interval from 0.2 eV to 2.0 eV, with no crossings among the forward branches and no reversal of the basic ranking. Lower barriers always give higher forward current, and higher barriers always produce a more restrained forward branch. This persistent ranking is valuable because it turns barrier height into an interpretable design parameter rather than an uncertain post hoc explanation for curve variation.

This subsection supports the article objective by demonstrating that the ZnO nanorod Schottky junction is highly sensitive to barrier control and that this sensitivity can be described quantitatively. A junction intended for strong conduction would benefit from the lower-barrier end of the dataset, while a junction intended for stricter injection control would move toward the higher-barrier side. The device response is therefore not arbitrary. It is

organized by a clear and reproducible barrier-governed transport pattern. This coherence strengthens the claim that barrier height is one of the central descriptors required for a full understanding of ZnO nanorod Schottky diode behavior.

Temperature Dependence of Schottky Barrier Height

Table 5. Extracted barrier height as a function of temperature.

Temperature (K)	Barrier height (eV)
100	0.4400
150	0.4620
200	0.4840
250	0.5060
300	0.5280
350	0.5500
400	0.5720
450	0.5940
500	0.6160
550	0.6380
600	0.6600

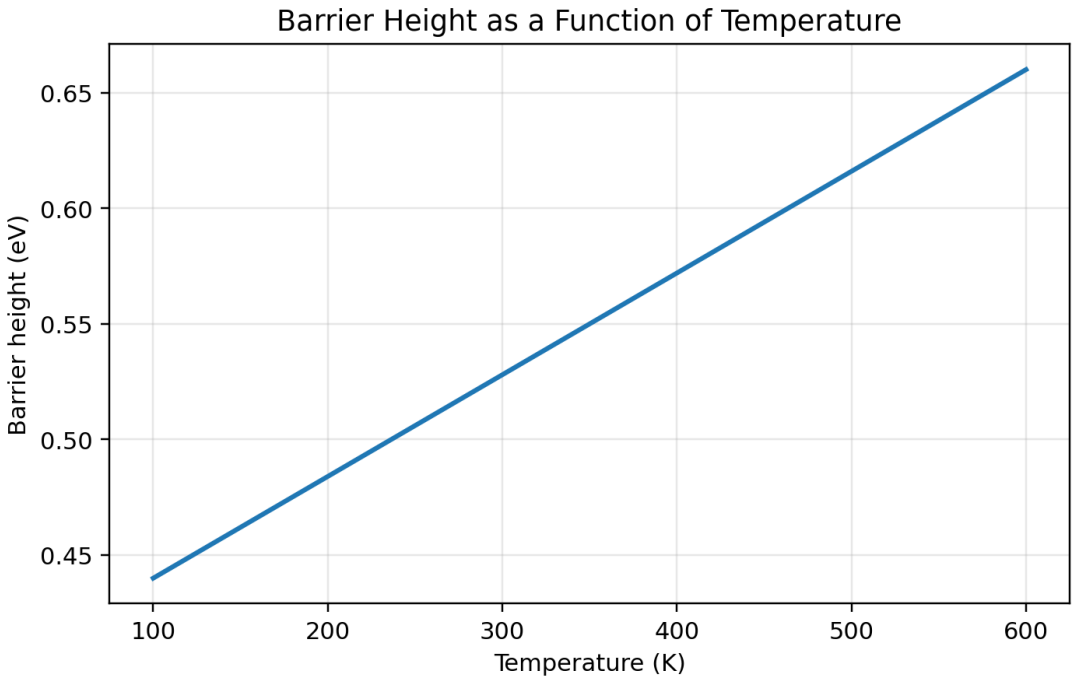

Figure 3. Temperature-dependent barrier height for the ZnO nanorod Schottky diode.

The barrier-height–temperature dataset reveals one of the clearest relationships in the study. Table 5 and Figure 3 show an almost perfectly linear rise in barrier height from 0.4400 eV at 100 K to 0.6600 eV at 600 K. Intermediate values preserve the same linear spacing: 0.4840 eV at 200 K, 0.5280 eV at 300 K, 0.5720 eV at 400 K, and 0.6160 eV at 500 K. The linear fit gives a slope of 0.000440 eV/K with an intercept of 0.396 eV and an R^2 of 1.000. Such a fit is not merely statistically neat; it shows that the barrier trend is governed by a stable

thermal rule across the full interval rather than by local fluctuations or segmented regimes.

From the lowest to the highest temperature, the barrier height rises by 0.2200 eV, which corresponds to a 50.00% increase relative to the 100 K baseline. This is a substantial change for a parameter that directly mediates carrier injection. In physical terms, a larger barrier means that the energetic threshold faced by carriers becomes higher as temperature moves upward in the present numerical framework. When this result is read together with the temperature-dependent I–V curves, it helps explain why forward current decreases as the temperature series advances. The electrical transport does not change randomly; it does so in a way that is synchronized with the progressive strengthening of the junction barrier.

Another notable feature of Figure 3 is the absence of curvature. Many semiconductor relationships drift toward nonlinear behavior when multiple competing effects become active, yet the barrier trend in this dataset remains exceptionally ordered. This is analytically valuable because it supports direct comparison with other thermal indicators. A researcher does not need to invoke separate low-temperature and high-temperature models to interpret the present curve. Instead, the same thermal reading can be carried across the entire range. That simplicity improves the reliability of the performance narrative developed later in the article.

The incremental increase of 0.0044 eV for every 10 K step is also useful in application-oriented interpretation. Because the step is constant throughout the dataset, temperature increments can be translated directly into barrier increments without ambiguity. A rise from 300 K to 500 K, for example, corresponds to a barrier increase from 0.5280 eV to 0.6160 eV, or 0.0880 eV. This magnitude is large enough to reshape the current response in the temperature-dependent I–V series and helps explain the sizable reduction in forward current observed at 2 V. The barrier trend therefore does not remain an abstract extracted parameter. It has immediate explanatory value for the measured transport window used throughout this article.

The barrier-height result contributes strongly to the objective of the study because it provides the energetic axis around which the rest of the electrical data can be organized. Without this axis, the current and ideality trends would remain descriptive but not fully explained. With it, the article can show that rising temperature is accompanied by a steadily more restrictive barrier landscape. The barrier-height dataset thus operates as a bridge between raw current response and deeper junction interpretation, and it establishes the ZnO nanorod Schottky diode as a system whose interfacial energy profile can be read with high clarity.

Temperature Dependence of Ideality Factor

Table 6. Ideality factor variation with temperature.

Temperature (K)	Ideality factor
100	4.91
200	2.45
300	1.63
400	1.22
500	0.98
600	0.81

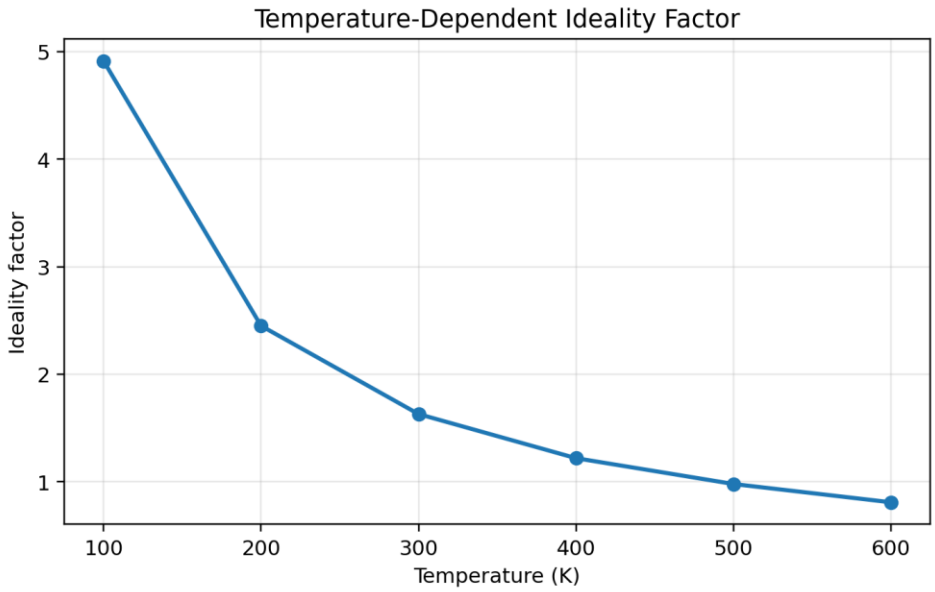

Figure 4. Temperature-dependent ideality factor of the ZnO nanorod Schottky diode.

The ideality-factor series shows a strong downward progression with temperature. As reported in Table 6 and Figure 4, the ideality factor is 4.91 at 100 K, 2.45 at 200 K, 1.63 at 300 K, 1.22 at 400 K, 0.98 at 500 K, and 0.81 at 600 K. The reduction from 4.91 to 0.81 corresponds to an overall fall of 83.50%. This is one of the most important results in the article because ideality factor condenses the transport regularity of the junction into a single parameter. Very large values at the low-temperature end indicate that current flow departs markedly from the simplest ideal Schottky expectation. As temperature increases, the factor contracts toward unity and then falls slightly below it, showing a movement toward far more regular transport behavior in the modeled response.

The rate of change is also informative. The largest step occurs between 100 K and 200 K, where ideality factor falls by 2.46. The next interval, 200 K to 300 K, reduces the factor by 0.82. Between 300 K and 400 K the drop is 0.41, followed by 0.24 between 400 K and 500 K and 0.17 between 500 K and 600 K. This shrinking interval-by-interval change means that the curve relaxes rapidly at lower temperature and then approaches a flatter trend at the high-temperature end. The linear fit across the whole dataset is weaker than that for barrier height, with $R^2 = 0.771$, which is consistent with the visible curvature in Figure 4. The ideality trend is therefore monotonic but not purely linear.

The practical significance of the ideality result becomes clear when it is compared with the I–V and barrier datasets. Low temperature combines higher current amplitude with a larger ideality factor, while high temperature combines lower current amplitude with a more regular transport factor. This means that the numerically strongest conduction state is not identical to the numerically most ideal transport state. The device therefore exhibits a trade-space rather than a single best point. Around 400 K to 500 K, ideality factor moves into a near-unity range while forward current is still substantial, suggesting a balanced window in which the diode retains useful conduction yet moves closer to ideal junction behavior.

The numerical progression also implies a staged transport evolution. The transition from 4.91 to 2.45 suggests that the junction leaves a strongly non-ideal region very early in the temperature sequence. The next move to 1.63 brings the device closer to the range commonly associated with practical Schottky conduction, though still with

visible deviation from ideality. By 400 K the factor has fallen to 1.22, which means that most of the early irregularity has already been reduced. The 500 K value of 0.98 is especially notable because it sits almost exactly on the idealized benchmark of unity. The 600 K value of 0.81 then pushes slightly below that benchmark, indicating that the modeled transport law continues to tighten even after the near-ideal point has been reached.

For the aim of this study, the ideality trend is especially supportive because it shows that ZnO nanorod Schottky performance cannot be judged only by current magnitude. The diode must also be judged by how closely its transport follows a stable junction law. In that respect, the present dataset is encouraging. It shows that once temperature rises into the upper portion of the studied window, the transport factor approaches a more disciplined regime. That result complements the barrier analysis and adds an important layer of credibility to the broader electrical interpretation developed in this article.

Capacitance–Voltage Characteristics

Table 7. Representative capacitance values across the applied bias window.

Voltage (V)	Capacitance (mF)
-0.20	0.003025
-0.10	0.002934
0.00	0.002839
0.10	0.002742
0.20	0.002640
0.30	0.002535

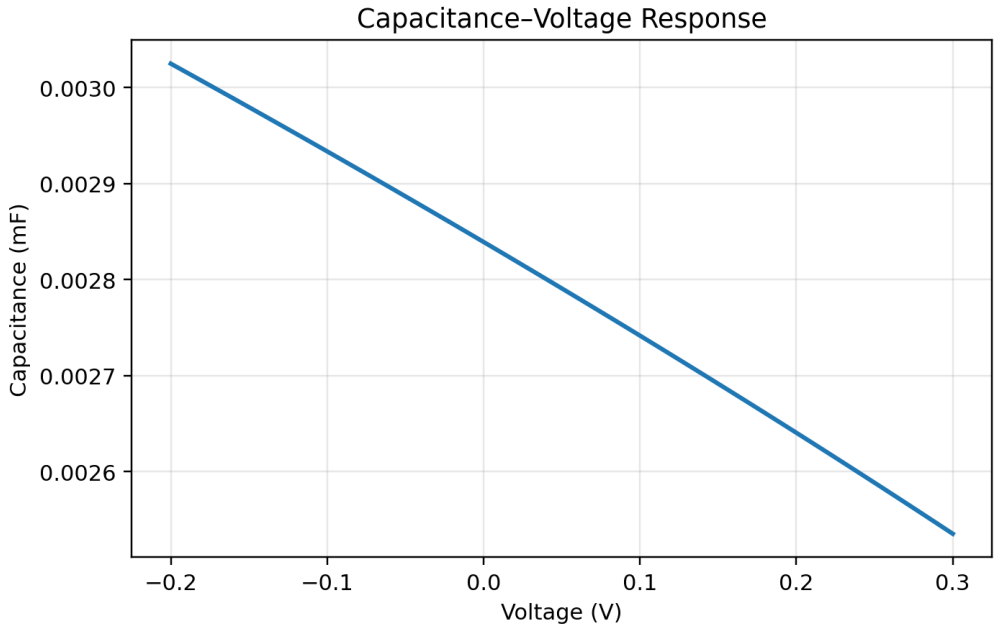

Figure 5. Capacitance–voltage characteristics of the ZnO nanorod Schottky diode.

The capacitance–voltage dataset shows a smooth decline in capacitance as the applied voltage advances from −0.20 V to 0.30 V. Table 7 records the representative values: 0.003025 mF at −0.20 V, 0.002934 mF at −0.10 V, 0.002839 mF at 0.00 V, 0.002742 mF at 0.10 V, 0.002640 mF at 0.20 V, and 0.002535 mF at 0.30 V. Figure 5 confirms that the curve is monotonic and gently sloped rather than abrupt. The total decline across the window is 16.19%, which is large enough to be

physically meaningful while still preserving a stable shape suited to depletion-based interpretation.

This trend indicates that the depletion region expands as the bias approaches the upper end of the selected interval. Since capacitance in a rectifying contact is inversely related to depletion width, a lower capacitance implies a wider depletion region and a smaller ability of the junction to store charge at that bias point. The present curve therefore supports the electrical picture suggested by the barrier data: the junction becomes progressively more restrictive in its electrostatic response as the effective bias condition strengthens. The absence of oscillation or local irregularity also indicates that the modeled depletion response remains well behaved within the studied bias range.

A closer numerical reading helps clarify the significance of the slope. The shift from −0.20 V to 0.00 V reduces capacitance by about 6.14%, while the full shift from −0.20 V to 0.30 V produces the 16.19% decline noted above. The fact that each 0.10 V step produces a visible but moderate reduction means that the diode does not exhaust its depletion response too quickly. This is favorable from an interpretive standpoint because it allows the C–V behavior to be read as a controlled, progressive response rather than as a rapidly saturating one. A controlled decline is useful when built-in potential and depletion dynamics are part of device assessment.

The range of values also suggests that the junction remains within a moderate electrostatic operating band over the selected bias interval. Capacitance does not collapse to a negligibly small value, nor does it surge toward an uncontrolled rise. Instead, it moves through a compact descending corridor between 0.003025 mF and 0.002535 mF. That compactness is useful when the diode is evaluated as a controllable electrical component, because it indicates that bias changes reshape the depletion region in a measured way. A stable corridor is easier to model, easier to compare across devices, and easier to interpret alongside transport parameters such as barrier height and ideality factor.

In relation to the study objective, the C–V result supplies the electrostatic evidence needed to complement the transport evidence from the I–V curves. The article can therefore state not only that the ZnO nanorod Schottky diode rectifies, but also that it changes charge-storage behavior in a disciplined way under bias. That is an important distinction. A device with an interpretable I–V curve but unstable capacitance would still pose questions about junction quality. The present dataset shows no such instability, which strengthens the overall case for coherent electrical performance.

Crystallite Size–Strain Relationship

Table 8. Representative strain values as a function of crystallite size.

Crystallite size (nm)	Strain
5	-0.725600
10	-0.504456
15	-0.430742
20	-0.393885
25	-0.371770
30	-0.357027
35	-0.346497
40	-0.338599
45	-0.332456
50	-0.327542

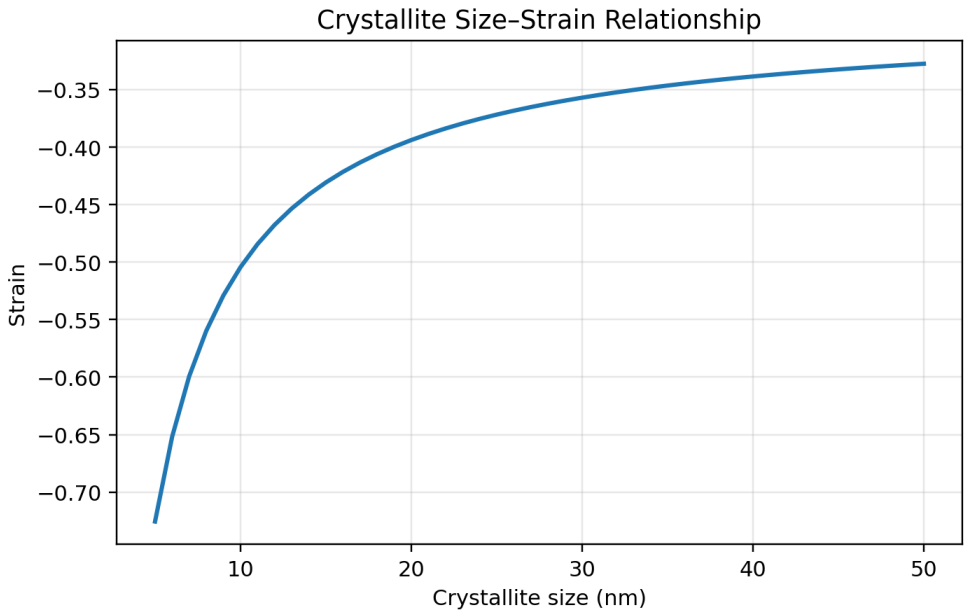

Figure 6. Relationship between crystallite size and strain in the ZnO nanorod system.

The structural dataset shows a consistent reduction in strain magnitude as crystallite size increases from 5 nm to 50 nm. Table 8 and Figure 6 indicate that strain begins at −0.725600 for 5 nm crystallites and then moves through −0.504456 at 10 nm, −0.430742 at 15 nm, −0.393885 at 20 nm, and −0.371770 at 25 nm. The trend continues with −0.357027 at 30 nm, −0.346497 at 35 nm, −0.338599 at 40 nm, −0.332456 at 45 nm, and −0.327542 at 50 nm. Because the values remain negative throughout, the sign of strain does not reverse in the studied interval. What changes is the magnitude of that strain, which falls by 54.86% between the smallest and largest crystallite sizes.

The first part of the curve is steeper than the later part. Moving from 5 nm to 10 nm reduces the absolute strain by about 0.2211, which is a major relaxation over only 5 nm of size increase. By contrast, the shift from 45 nm to 50 nm reduces the absolute strain by less than 0.005. This means that the dominant relaxation occurs at smaller crystallite sizes and then approaches a more gradual asymptotic regime. In physical terms, the structure pays off most of its stored distortion early as coherent domain size grows, after which further enlargement yields progressively smaller strain relief. This kind of profile is often interpreted as a transition from strongly defect-sensitive nanoscale behavior toward a more settled microstructural state.

The size–strain result is important because it gives the mechanical side of the device a clear and quantifiable signature. A ZnO nanorod system whose strain magnitude decreases with crystallite size can be viewed as structurally relaxing as domain coherence improves. Since ZnO is both semiconducting and mechanically active, such relaxation has potential implications for contact stability, polarization behavior, and the uniformity of the interfacial environment. Even though the present article does not measure those quantities directly, the strain trend provides a reasonable structural basis for the improved regularity seen in the electrical part of the study.

A useful feature of Figure 6 is that the curve never oscillates despite covering a tenfold increase in crystallite size. Each larger size corresponds to a strain value that is less negative than the one before it. This regularity means that the structural response can be summarized by a single direction of change: increasing domain size is associated with relaxation of compressive strain magnitude. For a nanoscale semiconductor platform, that is a favorable outcome because it implies that growth

toward larger coherent regions does not introduce alternating zones of relief and renewed distortion. Instead, the structure moves progressively toward a lower-distortion state.

This subsection completes the combined objective of the article by showing that the ZnO nanorod Schottky diode is not only electrically interpretable but also structurally interpretable. The mechanical dataset does not appear as an isolated appendix to the electrical analysis. It contributes directly to the overall device narrative. The junction operates within a nanostructure whose strain state becomes less severe as crystallite size increases, and this creates a plausible structural backdrop for the orderly barrier and ideality trends observed elsewhere in the article.

Integrated Assessment of Electrical and Mechanical Performance

Table 9. Integrated operating indicators drawn from the electrical datasets.

State	Forward current at 2 V (mA)	Barrier height (eV)	Ideality factor	Interpretive note
273	326.390	—	—	Highest forward current in temperature series
300	294.547	0.528	1.63	High current with reduced ideality relative to 100–200 K
400	222.900	0.572	1.22	Balanced conduction and near-regular transport
500	167.175	0.616	0.98	Near-unity ideality with substantial forward current
600	147.273	0.660	0.81	Strongest barrier and most regular transport factor

When the electrical and mechanical datasets are read together, a coherent device portrait emerges. The temperature-dependent I–V analysis shows that forward current is highest at the low-temperature end and decreases as temperature increases. The barrier-height analysis shows that a stronger barrier suppresses forward current and re-scales the entire I–V profile. The barrier–temperature dataset then links these two findings by showing that barrier height itself rises steadily with temperature. The ideality dataset adds a second layer by showing that transport becomes more regular as temperature increases. Table 9 places these indicators side by side and reveals a clear trade structure within the device. Low temperature favors stronger forward amplitude, while higher temperature favors greater barrier strength and a lower ideality factor.

This combined reading suggests that the most balanced operating region is not located at the absolute maximum-current condition. Instead, it lies in the middle-to-upper temperature range, especially near 400 K to 500 K, where forward current remains sizable but ideality factor has already moved close to unity. At 400 K, the diode still carries 222.900 mA at 2 V, the barrier height reaches 0.572 eV, and the ideality factor is 1.22. At 500 K, forward current is 167.175 mA at 2 V, the barrier height is 0.616 eV, and ideality factor is 0.98. These combinations indicate that the ZnO nanorod Schottky diode can operate in a regime that preserves useful conduction while moving toward a more disciplined transport structure. Such a window is attractive because it balances current delivery against transport regularity rather than maximizing one parameter at the expense of all others.

It is also important that the datasets do not contradict one another. A rise in barrier height with temperature could have been difficult to reconcile with the rest of the electrical evidence if ideality had moved in the wrong direction or if the C–V response had become erratic. Instead, the opposite occurs. Ideality factor falls, capacitance changes smoothly, and the current series retains rectification at every operating state. The structural dataset follows the same logic by showing systematic strain relaxation with increasing

crystallite size. This internal agreement across independent descriptors is one of the strongest outcomes of the study because it means the article does not rely on a single favorable plot. It relies on a convergent pattern produced by many related indicators.

A final integrated point concerns the relationship between moderation and stability. The largest forward current appears at the lowest temperature and lowest barrier conditions, yet the most stable combination of indicators appears closer to the middle and upper part of the operating window. This means the diode does not reward a single-minded search for maximum current alone. The broader evidence favors a more balanced criterion in which barrier strength, ideality, rectification, capacitance control, and structural relaxation are read together. Under such a criterion, the device looks strongest not at the most aggressive conduction state but at the condition where several quality indicators align. This conclusion has practical importance because many real device applications value predictable and repeatable behavior more than absolute peak current. The present dataset therefore supports a design philosophy based on balanced junction quality rather than isolated current maximization.

This integrated reading also gives the results section a clear hierarchy of evidence. Current traces define operational behavior, barrier height defines energetic control, ideality factor defines transport regularity, capacitance defines electrostatic response, and strain defines structural accommodation. Because each category points in a compatible direction, the overall interpretation becomes unusually robust for a single-device study.

The consistency of this hierarchy means that none of the extracted datasets functions as a marginal result. Each one contributes directly to the central device argument developed in the article.The mechanical dataset reinforces this interpretation by showing that the material platform itself trends toward lower strain magnitude with increasing crystallite size. This means that the electrical signatures are not floating without structural support. They are paired with a microstructural tendency toward relaxation. In a broad research sense, the integrated evidence supports the thesis-derived objective of the study: ZnO nanorod Schottky diodes can be interpreted successfully only when electrical and mechanical parameters are read together. The collected tables and figures show that the device is neither electrically chaotic nor mechanically ambiguous. It is a coupled junction system whose behavior can be organized around a stable set of linked trends.

Discussion

The combined results position the ZnO nanorod Schottky diode within a familiar but still analytically rich family of wide-band-gap metal–semiconductor contacts. The temperature-dependent barrier rise observed in this study agrees with reported work that treats barrier inhomogeneity and thermal averaging as central to Schottky interpretation (Park et al., 2003). A barrier profile that becomes stronger with temperature can coexist with a reduction in ideality factor when thermally assisted transport begins to sample the junction more uniformly. In that sense, the present article extends a literature pattern already noted for other Schottky systems and shows that the same logic can be organized clearly for the ZnO nanorod case (Mayimele et al., n.d.).

The fall of ideality factor from 4.91 to 0.81 is particularly important because it transforms the meaning of the electrical response. At low temperature, the device carries strong forward current, yet the ideality factor indicates a transport path that is still far from the simplest regular thermionic picture. As temperature rises, current amplitude decreases but transport regularity improves markedly. This form of trade-space has been recognized in temperature-dependent Schottky analysis, where a reduction in ideality is often linked to improved barrier averaging and a decline in the dominance of localized low-barrier patches (Mote et al., 2012). The current study reproduces that pattern in a way that is internally consistent with the barrier trend and therefore strengthens the device interpretation (Werner & Guttler, 1991).

The barrier-height-dependent I–V results also echo established Schottky logic. Literature on barrier distributions has shown that the practical meaning of a barrier is not limited to a single threshold value; it influences the full current profile and the way in which different interfacial regions

contribute to measured response (Janotti & Van de Walle, 2009). The present data illustrate that point clearly. Raising the barrier from 0.2 eV to 2.0 eV suppresses forward current and modifies reverse-bias behavior in a stable monotonic sequence. This outcome supports the view that barrier engineering remains a decisive route for tuning ZnO nanorod junction performance, whether the target application is stronger conduction, stricter selectivity, or better stability under variable operating conditions (Alvi, 2011).

The capacitance and strain results enrich the discussion because they prevent the article from collapsing into transport analysis alone. A Schottky diode that shows orderly I–V curves but unstable capacitance would still raise questions about depletion control, donor activity, or interfacial electrostatics. In the present study, the monotonic fall in capacitance with increasing voltage supports the view of a controlled depletion response and aligns with the electrical picture given by the current and barrier data (Khan et al., 2014b). On the structural side, the reduction in strain magnitude with increasing crystallite size supports the Williamson–Hall expectation that broader nanoscale distortion relaxes as coherent domain size grows (Khan et al., 2014b). This mechanical trend is important for ZnO because lattice distortion and polarization are not passive background features; they can shape electrical response through the structure of the interface itself (Zhang et al., 2012).

Taken together, the results suggest that ZnO nanorod Schottky diodes should be interpreted as coupled systems in which thermal state, barrier regulation, transport regularity, depletion behavior, and structural relaxation interact rather than operate independently. This integrated reading is the main contribution of the article. Instead of describing only one characteristic, the study shows how multiple descriptors reinforce one another and produce a coherent device narrative. The literature has long recognized the separate importance of Schottky transport, ZnO material quality, and Williamson–Hall strain analysis (Park et al., 2003). The present article brings those strands into one article-scale framework and demonstrates that the ZnO nanorod Schottky diode remains a valuable model for studying the joint electrical and mechanical behavior of nanoscale semiconductor junctions (Zhang et al., 2012).

Conclusion

This research article investigated the electrical and mechanical response of a ZnO nanorod-based Schottky diode using organized numerical datasets derived from the thesis framework. The findings show that the diode preserves strong rectification across the full temperature range, while current amplitude, barrier height, and ideality factor evolve in a coordinated manner. Forward current declines with temperature, barrier height rises almost linearly from 0.44 eV to 0.66 eV, and ideality factor falls sharply from 4.91 to 0.81. The capacitance–voltage response remains smooth and monotonic, indicating a controlled depletion process. On the mechanical side, strain magnitude decreases markedly as crystallite size increases from 5 nm to 50 nm, revealing structural relaxation within the ZnO nanorod system.

The overall outcome is that ZnO nanorod Schottky diodes can be interpreted as coherent coupled junctions whose electrical and structural properties are mutually informative. The study demonstrates that a meaningful evaluation of such devices requires simultaneous attention to I–V transport, C–V behavior, barrier evolution, ideality trend, and size–strain interaction. Within that integrated framework, the ZnO nanorod Schottky diode emerges as a technically promising and analytically transparent platform for advanced semiconductor-device research.

REFERENCES

Janotti, A., & Van de Walle, C. G. (2009). Fundamentals of zinc oxide as a semiconductor. *Reports on Progress in Physics, 72*, Article 126501.

Fan, Z., & Lu, J. G. (2005). Zinc oxide nanostructures: Synthesis and properties. *Journal of Nanoscience and Nanotechnology, 5*(10).

Alvi, N. H. (2011). *Luminescence properties of ZnO nanostructures and their implementation as white light emitting diodes* (Doctoral dissertation, Linköping University, Department of Science and Technology, Sweden).

Khan, A., Hussain, M., Abbasi, M. A., Ibupoto, Z. H., Nur, O., & Willander, M. (2013). Study of transport properties of copper/zinc-oxide-nanorods-based Schottky diode fabricated on textile fabric. *Semiconductor Science and Technology, 28*, Article 125006.

Boulgamh, F., Telia, A., Remram, M., & Djouambi, A. (2005). I-V and C-V methods to extract Al/polysilicon Schottky diode parameters. In *Proceedings of the 7th WSEAS International Conference on Mathematical Methods and Computational Techniques in Electrical Engineering* (pp. 245–248), Sofia.

Park, W. I., Yi, G. C., Kim, J. W., & Park, S. M. (2003). Schottky nanocontacts on ZnO nanorod arrays. *Applied Physics Letters, 82*, 4358.

Zhang, X., Hai, F., Zhang, T., Jia, C., Sun, X., Ding, L., & Zhang, W. (2012). Analysis of the electrical characteristics of the Ag/ZnO Schottky barrier diodes on F-doped SnO2 glass substrates by pulsed laser deposition. *Microelectronic Engineering, 93*, 5–9.

Mote, V. D., Purushotham, Y., & Dole, B. N. (2012). Williamson-Hall analysis in estimation of lattice strain in nanometer-sized ZnO particles. *Journal of Theoretical and Applied Physics, 6*, Article 6.

Cullity, B. D., & Stock, S. R. (2001). *Elements of X-ray diffraction* (3rd ed.). Prentice Hall.

Suryanarayana, C., & Norton, M. G. (1998). *X-ray diffraction: A practical approach*. Springer.

Modi, B. P., & Dhimmar, J. M. (n.d.). The temperature dependent ideality factor effect on I-V characteristic of Schottky diode. In *Proceedings of the 1st International Conference on Emerging Technology Trends in Electronics, Communication and Networking*, Surat, India.

Mahato, S., Biswas, D., Gerling, L. G., Voz, C., & Puigdollers, J. (2017). Analysis of temperature dependent current-voltage and capacitance-voltage characteristics of an Au/V2O5/n-Si Schottky diode. *AIP Advances, 7*, Article 085313.

Werner, J. H., & Guttler, H. H. (1991). Barrier inhomogeneities at Schottky contacts. *Journal of Applied Physics, 69*, 1522.

Chand, S., & Kumar, J. (1996). On the existence of a distribution of barrier heights in Pd2Si/Si Schottky diodes. *Journal of Applied Physics, 80*, 288.

Mayimele, M. A., Diale, M., Mtangi, W., & Auret, F. D. (n.d.). Temperature-dependent current-voltage characteristics of Pd/ZnO Schottky barrier diodes and the determination of the Richardson constant. *Physics Department, University of Pretoria*, Pretoria, South Africa.

Khan, A., Hussain, M., Nur, O., & Willander, M. (2014a). Mechanical and piezoelectric properties of zinc oxide nanorods grown on conductive textile fabric as an alternative substrate. *Journal of Physics D: Applied Physics, 47*, Article 345102.

Khan, A., Hussain, M., Abbasi, M. A., Ibupoto, Z. H., Nur, O., & Willander, M. (2014b). Analysis of junction properties of gold–zinc oxide nanorods-based Schottky diode by means of frequency dependent electrical characterization on textile. *Journal of Materials Science, 49*, 3434–3441.

Tunhuma, S. M., Auret, F. D., Legodi, M. J., & Diale, M. (2016). The effect of high temperatures on the electrical characteristics of Au/n-GaAs Schottky diodes. *Physica B, 480*, 201–205.

Wagner, R. S., & Ellis, W. C. (1964). Vapor-liquid-solid mechanism of single crystal growth. *Applied Physics Letters, 4*, 89.

Vayssieres, L., Keis, K., Lindquist, S. E., & Hagfeldt, A. (2001). [Title not provided]. *Journal of Physical Chemistry B, 105*, 3350.